Hydrol. Earth Syst. Sci. Discuss., 11, 9829–9862, 2014
www.hydrol-earth-syst-sci-discuss.net/11/9829/2014/
doi:10.5194/hessd-11-9829-2014

Hydrology and Earth System Sciences
Open Access
Discussions

Impact of flow velocity on biochemical processes – a laboratory experiment

A. Boisson[1,*], **D. Roubinet**[1,**], **L. Aquilina**[1], **O. Bour**[1], **and P. Davy**[1]

[1]Géosciences Rennes, CNRS – UMR6118, Université de Rennes 1, Rennes, France
[*]now at: BRGM, D3E/NRE, Indo-French Centre for Groundwater Research, 500 007 Hyderabad, India
[**]now at: Applied and Environmental Geophysics Group, University of Lausanne, 1015 Lausanne, Switzerland

Received: 9 July 2014 – Accepted: 31 July 2014 – Published: 20 August 2014

Correspondence to: A. Boisson (a.boisson@brgm.fr)

Published by Copernicus Publications on behalf of the European Geosciences Union.

Abstract

Understanding and predicting hydraulic and chemical properties of natural environments are current crucial challenges. It requires considering hydraulic, chemical and biological processes and evaluating how hydrodynamic properties impact on biochemical reactions. In this context, an original laboratory experiment to study the impact of flow velocity on biochemical reactions along a one-dimensional flow streamline has been developed. Based on the example of nitrate reduction, nitrate-rich water passes through plastic tubes at several flow velocities (from 6.2 to 35 mm min^{-1}), while nitrate concentration at the tube outlet is monitored for more than 500 h. This experimental setup allows assessing the biologically controlled reaction between a mobile electron acceptor (nitrate) and an electron donor (carbon) coming from an immobile phase (tube) that produces carbon during its degradation by microorganisms. It results in observing a dynamic of the nitrate transformation associated with biofilm development which is flow-velocity dependent. It is proposed that the main behaviors of the reaction rates are related to phases of biofilm development through a simple analytical model including assimilation. Experiment results and their interpretation demonstrate a significant impact of flow velocity on reaction performance and stability and highlight the relevance of dynamic experiments over static experiments for understanding biogeochemical processes.

1 Introduction

Worldwide leaching of agricultural-derived nitrate to groundwater represents a long-term risk for groundwater quality (Khan and Spalding, 2004; Spalding and Exner, 1993). In this context, natural attenuation of this compound by denitrification has been extensively studied from the batch scale (Kornaros and Lyberatos, 1997; Marazioti et al., 2003) to the aquifer scale (Clément et al., 2003; Korom, 1992; Tarits et al., 2006). However, a full understanding of denitrification processes in natural systems requires

HESSD
11, 9829–9862, 2014

a structural description of the interactions between hydraulic, chemical and biological processes at several spatial and temporal scales (Sturman et al., 1995). Whereas the understanding of reaction kinetics is well developed for static experiments (Hiscock et al., 1991; Korom, 1992), their understanding for dynamic experiments needs further development and is critical as reactivity in complex natural media is partially driven by hydraulic heterogeneities (Tompkins et al., 2001). Effects of hydraulic heterogeneities have been studied on reactive columns (Sinke et al., 1998; von Gunten and Zobrist, 1993) or on simple geometries such as pore networks (Thullner et al., 2002) and tubes (De Beer et al., 1996; Garny et al., 2009; Lewandowski et al., 2007), and these studies are devoted to biofilm development related to reactivity processes (De Beer et al., 1996; Garny et al., 2009; Lewandowski et al., 2007) or hydraulic parameters (Beyenal and Lewandowski, 2000; Garny et al., 2009; Lau and Liu, 1993; Stoodley et al., 1994). Whereas the latter studies focus on conduit reactors at the centimeter scale (length and diameter/thickness) with large flow velocities (10^2–10^3 mm min^{-1}), Characklis (1981) offers a global discussion on the influence of hydraulic conditions on biofilm development (shape, size and reactive layer) and nutrient availability. However, there is a lack of knowledge about the direct impact of fluid velocity on bulk reactivity associated with biochemical reactions. The latter aspect is critical as flow velocity may be a key-controlling parameter in systems where mobile water interacts with a growing non-mobile biological phase. This is particularly the case in aquifers where a broad range of flow velocity in pores and fractures is expected.

The global comprehension of hydrodynamic parameters' effects on bioreactivity requires an accurate understanding of their interactions at the laboratory scale. For this purpose, we propose an experiment in plastic tubes that are equivalent to 1-D flow systems where the geometry is perfectly known and the hydraulic parameters are well controlled. This is the most convenient configuration to assess the influence of hydrodynamic parameters, such as advection along a single flow line. In addition, it avoids dealing with the flow complexity of columns that are a sum of processes occurring on a large number of flow lines.

HESSD
11, 9829–9862, 2014

In the experiment presented in Sect. 2, the reactivity evolution of nitrate-rich water passing through PVC tubes is measured for different flow velocities. The hydrodynamic dependence of the experiment results is studied in Sect. 3 and the relationship between biofilm development and reaction processes is analyzed with a simple analytical model in Sect. 4. The impact of flow velocity on biofilm properties and reaction efficiency is then discussed in Sect. 5.

2 Experimental set-up

2.1 Experimental concept

In order to reproduce conditions where the electron acceptor is mobile with water and the electron donor comes from an immobile part, as it is the case for denitrification where nitrate flow with water and the electron donor (organic matter or minerals as pyrite) comes from the soil or rock matrix, we propose an original experiment for the study of biochemical reactions. Knowing that plastic compounds can serve as substrate for heterotrophic bacterial growth (Mohee et al., 2008; Shah et al., 2008), we set up an experiment where nitrate-rich water is in contact with "reactive" plastic tubes. In such an experiment, bacteria grow using carbon from the tubes and nitrates from the water reproducing denitrification process with well-controlled experimental conditions. Whereas column experiments are related to approximate equivalent parameters, the simple geometry of tube experiments enables us to know critical parameters such as the real flow velocity and the flow/carbon-source contact area. By applying slow flow velocities (from 6.2 to 35 mm min^{-1}) in small diameter tubes (2 mm), our experiment is a closer reproduction of pore-scale (or fracture-scale) phenomena than existing open channel experiments (Garny et al., 2009; Lewandowski et al., 2007). The presented plastic tube experiment is an original and convenient experimental set-up characterized by the control of key experimental parameters that are usually not well defined. Although this experiment does not reproduce a natural reaction, it is a good representation of possible

HESSD
11, 9829–9862, 2014

behavior between the mobile/immobile electron acceptor/donor during biochemical reactions that can occur in macropore soils or fractured aquifers. The water used in the following static and dynamic experiments has been collected in the Ploemeur site (Brittany, France) where natural denitrification has been observed (Tarits et al., 2006) and the velocities used for the dynamic experiment are in the range of the velocities estimated in the Ploemeur site as well. Note that this site has provided water to the city of Ploemeur since 1991 at a rate of 10^6 m^3 per year (Jiménez-Martínez et al., 2013; Leray et al., 2012) thanks to a contact zone between granite and schist (Ruelleu et al., 2010). It also appears to sustain natural denitrification that seems to be enhanced by flow dynamics of the aquifer (Tarits et al., 2006).

Preliminary static (or batch) experiments enable us to identify "reactive" plastic tubes that are able to release carbon to sustain heterotrophic development reactions. 150 mL of the water collected in the Ploemeur site (Brittany, France) is deoxygenated and placed in glass flasks under an argon atmosphere with (1) no plastic tubes, (2) Pharmed® and Teflon tubes, and (3) Watson Marlow® PVC double manifold tubes (named PVC tubes). Plastic tube fragments correspond to a mass of 8 g and a reactive surface of 0.018 m^2 and the experiments are conducted in duplicate that lead to similar results. Nitrate concentration evolves only for the PVC tube experiments where nitrates are completely consumed within 150 h with a production of organic carbon up to a concentration of 22.03 mg L^{-1} after 165 h (Fig. 1). Longer monitoring shows a release of organic carbon up to a concentration of 76.8 mg L^{-1} after 378 h. PVC tubes are thus the carbon source of the observed denitrification reaction that does not depend only on water compounds.

The medium inoculation occurs by bacterial attachment and we assume a complete biofilm behavior without considering the diversity of microbial populations and their interaction. Part of the developing microbial population could come from the tubes since no sterilization was done. Nevertheless, bacteria are supposed to mainly come from the water since (1) they are naturally present in such groundwater (Bekins, 2000; Bougon et al., 2009) and (2) several experiments of crushed granite and water from the

HESSD
11, 9829–9862, 2014

Ploemeur site, using the same water, have showed denitrification processes (Ayraud et al., 2006; Tarits et al., 2006).

2.2 Experimental conditions for dynamic experiments

After demonstrating the PVC tube reactivity with static experiments, dynamic experiments were conducted. The latter experiments consist of (1) continuously injecting nitrate-rich water in PVC tubes and (2) monitoring nitrate consumption due to bacterial development through nitrate and nitrite concentration measurements at the tube outlets. The reactive plastic tubes used for the experiments have an inner diameter of 2 mm and a length of 135 cm and new tubes are used for each experiment. These experiments are performed in the dark at a constant temperature of 18 °C and oxygen measurements are done daily.

The nitrate-rich water (45 mg L^{-1}) collected in the Ploemeur site (Brittany, France) was not treated before the experiments. Although the water coming from the same piezometer has been sampled at different dates within a year, no water chemistry changes have been observed during this period. This water is almost free of organic carbon with a concentration lower than 0.5 mg L^{-1}.

Prior to experimental use, the water is deoxygenated by Argon bubbling and then maintained in anoxic conditions under an argon atmosphere in a high-density polyethylene tank (whose non reactivity is controlled). The organic carbon concentration in the injected water remains below 0.5 ppm during the whole experiment.

The water delivered from the tank to the reacting PVC tubes passes through non-reactive Teflon and Pharmed tubes placed in a peristaltic pump (Watson Marlow®; Fig. 2) where the non-reactivity of the setup before the PVC tubes is checked during all the experiments. The experiments are performed at four different flow rates corresponding to the flow velocities v_1, v_2, v_3 and v_4 equal to 6.2, 11, 17 and 35 mm min^{-1}, respectively, and are conducted in triplicate for each flow velocity. Such velocities imply residence times in the tubes ranging from 40 min to 3 h and 40 min whereas the whole experiment lasts more than 500 h.

HESSD
11, 9829–9862, 2014

2.3 Analysis and methods

The experiments are monitored by a daily sampling of water inside the tank for the static experiments and at the outlet of the tubes for the dynamic experiments. All samples are filtered with a 45 µm Sartorius filter before analyses and major anions (NO_3^-, NO_2^-, SO_4^{2-}, Cl^- and F^-) are analyzed using a Dionex DX 120 ion chromatograph. Organic and inorganic carbons are analyzed every three days using a Shimadzu 5050A Total Organic Carbon analyzer. The volume used for analyses (5 mL) is equal to the full volume of the tube, here after named pore volume. It corresponds to a volume that passes only once through the system and leads to a sampling protocol independent of the flow velocity. Dissolved oxygen is measured using a WTW315i-CondOX probe and flow is measured daily by weighing at the tube outlet (its variations are below 2 % in weighed mass).

3 Experimental results

The nitrate consumption per unit of volume at time t is defined as

$$\Delta C_{NO_3^-}(t) = C^{IN}_{NO_3^-} - C^{OUT}_{NO_3^-}(t), \quad (1)$$

where $C^{IN}_{NO_3^-}$ (g L^{-1}) is the initial concentration in the flasks for the static experiments and the concentration measured at the tube inlet for the dynamic experiments, and $C^{OUT}_{NO_3^-}(t)$ (g L^{-1}) is the concentration measured at time t in the flasks for the static experiments and at the tube outlets for the dynamic experiments.

Figure 3 represents the nitrate consumption $\Delta C_{NO_3^-}(t)$ (Eq. 1) for the dynamic experiments where the results obtained with the flow velocities v_1, v_2, v_3 and v_4 are represented by full blue, dashed green, dashdot magenta and dotted red curves, respectively. The presented values correspond to the values averaged over three replicates.

HESSD
11, 9829–9862, 2014

All replicates show the same tendency and error bars represent the mean square deviation. Note that no evolution of the nitrate concentration in the tube inlet water has been observed from daily measurements. Therefore nitrates concentration at the tube inlet remains constant during the whole experiment (45 mg L^{-1}).

For static experiments (Fig. 1), nitrate concentration in the flask decreases until complete consumption. On the contrary, dynamic experiments (Fig. 3) are characterized by more complex reactive processes with first a linear increase of nitrate consumption that seems to not depend on the flow velocity (dashed black curve), followed by either a "relative" stabilization characterized by small variations (full blue and dotted red curves) or a decrease (dashed green and dashdot magenta curves). The dynamic of nitrate consumption seems thus to be limited by different processes for flow-through experiments. The identified phases are described in detail below and their relationship to the development of biofilm observed during the experiments (Fig. 4) is studied in the next section (Sect. 4).

3.1 Initiation of degradation processes (Phase 1)

The first phase (dashed black curve, Fig. 3) corresponds to a linear increase of nitrate consumption that is similar for the four flow velocities. Noticing that residence times within the tubes are flow-velocity dependent, identical concentration at the tube outlets corresponds to a greater reactivity for higher flow velocities.

In order to characterize the relationship between reactivity and the mass of nitrate brought into the system, we represent the nitrate reactivity evolution (in mg m^{-2} s^{-1}) with the number of pore volumes (Fig. 5). The similar main slope at the beginning of the experiments shows that the consumption (or degradation) rate of nitrates depends mainly on the quantity of water passed through the tubes (i.e. the number of pore volumes) and that flow velocity impacts only the final behavior of the reactivity. The mass of nitrate consumed per pore volume is thus independent of the residence time.

At the beginning of the experiment biofilm develops as clusters from the millimeter to the centimeter scale (Fig. 4a), and then spreads continuously along the tubes (Fig. 4b).

HESSD
11, 9829–9862, 2014

During this first phase, the increase of the degradation rate with time can therefore be related to biofilm development inside the tubes. As nitrate and organic carbon are present at the tube outlets (where carbon concentration ranges from 6.5 to 21 mg L^{-1}), they are in excess in the system and cannot be considered as limiting factors. The factor controlling this first phase for dynamic experiments is thus the bacterial growth rate leading to a total consumption of nitrate for the static experiments.

3.2 Stabilization and decrease (Phase 2)

The second phase (Fig. 3) is characterized either by a "relative stabilization" of nitrate consumption (full blue and dotted red curves) or by a strong decrease (dashed green and dashdot magenta curves). As carbon and nitrates (the main reactants) are still in excess at the tube outlets, their availability is not the limiting factor.

The transition from Phase 1 (described in the previous section) to Phase 2 depends on the flow velocity. It corresponds to the maximum nitrate consumption (Fig. 3) that can be reached for the three lowest velocities (full blue, dashed green and dashdot magenta curves). Concerning the fastest velocity v_4, the previously named "relative stabilization" corresponds to a succession of decreases and increases oscillating around a "relative threshold".

The nitrate reduction capacity during this phase seems to be controlled by the flow velocity that can impact biofilm properties. The following section is dedicated to explaining the latter experimental observations by relating them to biofilm properties. The two phases previously identified are linked to several steps of the biofilm development with specific flow-dependences.

HESSD
11, 9829–9862, 2014

4 Linking biofilm properties and reaction processes

From the measurements of nitrate and nitrite concentrations in both static and dynamic experiments, the present section aims to evaluate the biofilm properties and relate them to the observed reaction efficiency.

4.1 Evaluation of biofilm properties

4.1.1 Biofilm weight

Since the dynamic of biofilm development is likely important in the reaction rate evolution, we aim to evaluate the dynamic of produced biofilm mass during the experiments. Continuous monitoring and complete quantification of the biofilm were not possible during the experiment due to technical reasons. To counteract this problem, we propose to estimate the biofilm property evolution considering that the production of cells can be calculated using the method of McCarty (1972) in which the quantity of produced mass depends on the electron donor. For example, 0.24 g of cells is produced per gram NO_3-N removed for H_2 (Ergas and Reuss, 2001; Ergas and Rheinheimer, 2004), 0.64 g of cells in the case of sulfur (Sengupta and Ergas, 2006), and 0.45 and 1.21 g of cells in the case of methanol and acetic acid, respectively (Hamlin et al., 2008). Those authors consider that the usual range of heterotrophic denitrification is between 0.6 and 0.9 g of cells produced per gram of NO_3-N removed. In the present study, and for demonstration purposes, we consider the mean value of the previous range, corresponding to 0.75 g of cells produced per gram of NO_3-N removed, or 0.17 g of organic matter produced per gram of nitrate consumed.

Note that the main uncertainty is then about N gasses (N_2, NO) that are produced but not measured. However, the corresponding reaction given by Eq. (2) in the case of methanol (Hamlin et al., 2008) shows that, even if a considerable mass of cells can be produced in comparison to the mass of nitrate removed, only a small fraction of nitrogen is assimilated in the cell and most of it is reduced to N_2

HESSD
11, 9829–9862, 2014

$$NO_3^- + 1.08CH_3OH + H^+ \rightarrow 0.065C_5H_7O_2N + 0.47N_2 + 0.75CO_2 + 2.44H_2O. \quad (2)$$

Assuming that 1 g of consumed nitrate allows the production of 0.17 g of organic matter, we calculate the temporal evolution of the cumulative biofilm weight $\overline{m_{bio}}$ (g) from the NO_3 and NO_2 in and out fluxes as

$$\overline{m_{bio}}(t) = 0.17 \times M_{NO_3^-} \times \overline{n^{bio}_{NO_3^-}}(t), \quad (3)$$

where $M_{NO_3^-}$ ($g\,mol^{-1}$) is the molar mass of nitrate and $\overline{n^{bio}_{NO_3^-}}$ (mol) the total number of nitrate moles used for biofilm formation until time t. The latter quantity depends on the number of consumed nitrate moles $\overline{n^{cons}_{NO_3^-}}$ (mol) and produced nitrite moles $\overline{n^{prod}_{NO_2^-}}$ (mol) as

$$\overline{n^{bio}_{NO_3^-}}(t) = \overline{n^{cons}_{NO_3^-}}(t) - \overline{n^{prod}_{NO_2^-}}(t). \quad (4)$$

For our calculations, these molar quantities are deduced from nitrate and nitrite concentration measurements. Thus, the total number of nitrate moles used for biofilm formation until time t is expressed as follows.

For batch experiments:

$$\overline{n^{bio}_{NO_3^-}}(t) = \left\{ \frac{\left[C^{IN}_{NO_3^-} - C^{OUT}_{NO_3^-}(t)\right]}{M_{NO_3^-}} - \frac{C^{OUT}_{NO_2^-}(t)}{M_{NO_2^-}} \right\} \times V, \quad (5)$$

and for tube experiments:

HESSD
11, 9829–9862, 2014

$$\overline{n^{\text{bio}}_{\text{NO}_3^-}}(t) = \int_0^t \left\{ \frac{\left[C^{\text{IN}}_{\text{NO}_3^-} - C^{\text{OUT}}_{\text{NO}_3^-}(\tau) \right]}{M_{\text{NO}_3^-}} - \frac{C^{\text{OUT}}_{\text{NO}_2^-}(\tau)}{M_{\text{NO}_2^-}} \right\} \times q \, \mathrm{d}\tau, \quad (6)$$

where $C^{\text{IN}}_{\text{NO}_3^-}$ is the nitrate concentration defined in the previous section, $C^{\text{OUT}}_{\text{NO}_3^-}(t)$ and $C^{\text{OUT}}_{\text{NO}_2^-}(t)$ (g L^{-1}) are nitrate and nitrite concentrations, respectively, measured at time t in the batch volume (batch experiment) and at the tube outlets (tube experiments), $M_{\text{NO}_2^-}$ (g mol^{-1}) is the molar mass of nitrite, V (L) is the water volume for the batch experiment and q (L s^{-1}) the flow rate for the tube experiments.

Figure 6 shows the temporal evolution of biofilm properties characterized by the cumulative biofilm weight $\overline{m_{\text{bio}}}$ (in mg). The static input of the batch experiment (large black curve) implies a stronger increase of the biofilm weight than the dynamic input of the tube experiments (full blue, dashed green, dashdot magenta and dotted red curves). In addition, the batch experiment leads to a constant biofilm weight (last part of the black large curve) due to the total consumption of nitrate present in the batch volume.

At the end of the slowest experiment (velocity v_1), the biofilm has been extracted from the tube and its dry weight evaluated at 1.9 mg whereas the proposed model leads to a cumulative biofilm weight of 0.62 mg. Since this measurement is destructive, it can be done only once at the end of the experiment. This difference is likely due to the simplifications of the proposed model where potential biofilm loss by detachment or decay and addition of suspended materials and extracellular polymeric substances are not considered. Note that the latter phenomenon can increase the biofilm weight and that uncertainties remain concerning the relation linking cells produced per quantity of consumed nitrate. However, the present study aims to conduct a qualitative analysis of

HESSD
11, 9829–9862, 2014

the experimental results where we are particularly interested in the relative temporal evolution of the biofilm properties and in their link to the reaction efficiency.

4.1.2 Biofilm thickness

For comparison with previous studies, we evaluate the average biofilm thickness b_{bio} by considering that biofilm forms a uniform cylinder stuck on the tube wall:

$$b_{bio} = R - \sqrt{R^2 - V_{bio}/\pi L}, \quad (7)$$

where R is the radius of the tube, L the tube length and V_{bio} the biofilm volume. The latter is deduced from the biofilm mass $\overline{m_{bio}}$ (Eq. 3) assuming a biofilm mass density of 10 mg cm^{-3} (Williamson and McCarty, 1976). In order to obtain comparable results, the same geometry is assumed for static and dynamic experiments. Note that biofilm thickness gives the same qualitative information as the biofilm weight and is introduced here only for an easier comparison with existing studies.

As tube experiments are conducted for several flow velocities, the temporal evolution of biofilm is potentially impacted by both the effect of flow on biofilm structure and the mass of nutrient injected in the system over time. In order to focus on the interactions between flow and biofilm-structure properties, we study the biofilm evolution with the quantity of nutrient input N_{input} (g) defined as follow.

For batch experiments:

$$N_{input} = C^{IN}_{NO_3^-} \times V \quad (8)$$

and for tube experiments:

$$N_{input}(t) = C^{IN}_{NO_3^-} \times q \times t. \quad (9)$$

Figure 7 shows the evolution of the biofilm properties (characterized here by the biofilm thickness b_{bio}) with the quantity of nutrient input N_{input}. The batch experiment (large

HESSD
11, 9829–9862, 2014

black curve) leads to a fast consumption of nutrient because the small initial quantity of nutrient is not enriched by new inputs. Concerning the tube experiments, the presented results show that increasing the flow velocity leads to (1) smaller values of the biofilm thickness per nutrient input unit, and (2) a slower evolution of the biofilm growth along the quantity of injected nutrient. It implies that fast velocities result in a thinner (or less dense) "effective" biofilm, where "effective" means that the biofilm is assumed to be homogeneous and of the same density for all experiments. This biofilm thickness can also be interpreted as a "potential" thickness, as its estimate does not take into account possible erosion and/or detachment processes.

By relating biofilm growth to the nitrate transformation rate, the next section aims to characterize how the evolution of biofilm properties is related to the flow velocity and how the latter flow velocity impacts the reaction efficiency.

4.2 Linking biofilm growth and nitrate transformation

In order to illustrate the flow-dependent heterogeneity of biofilm structures and its potential role on nitrate transformation, we calculate the rate of nitrate transformation V_{trans} ($\text{mg m}^{-2}\,\text{s}^{-1}$) and compare it to our estimate of biofilm thickness.

For the batch experiment, V_{trans} is defined as

$$V_{\text{trans}}(t) = \frac{\Delta C^{\text{bio}}_{NO_3^-}}{\Delta t} \times \frac{V}{S} \tag{10}$$

where $\Delta C^{\text{bio}}_{NO_3^-}$ (g L^{-1}) is the concentration of nitrate transformed in biofilm during the time interval Δt and S is the reactive PVC surface in the batch and tube experiments. Note that the rate of nitrate transformation (Eq. 10) and nitrate reactivity (Fig. 5) differ as the first one considers only the nitrate contributing to biofilm growth (assimilation) whereas the second one considers all the consumed nitrate (reduction).

HESSD
11, 9829–9862, 2014

The value of $\Delta C^{bio}_{NO_3^-}$ at time t_i is evaluated by the following expression for the batch experiment:

$$\Delta C^{bio}_{NO_3^-}(t_i) = \left[n^{bio}_{NO_3^-}(t_i) - n^{bio}_{NO_3^-}(t_{i-1}) \right] \times M_{NO_3^-} \quad (11)$$

where $n^{bio}_{NO_3^-}(t_i)$ (mol L^{-1}) is the number of moles transformed in biofilm per unit of volume until time t_i and is expressed as

$$n^{bio}_{NO_3^-}(t_i) = \frac{C^{IN}_{NO_3^-} - C^{OUT}_{NO_3^-}(t_i)}{M_{NO_3^-}} - \frac{C^{OUT}_{NO_2^-}(t_i)}{M_{NO_2^-}}. \quad (12)$$

For the tube experiments, the interval time Δt of expression 10 is set at the time required to travel along the tube by advection (from its inlet to its outlet) and leads to the following expression

$$V_{trans}(t) = \Delta C^{bio}_{NO_3^-} \times \frac{q}{S} \quad (13)$$

where $\Delta C^{bio}_{NO_3^-}$, the concentration of nitrate contributing to biofilm formation during the interval time Δt, is expressed as

$$\Delta C^{bio}_{NO_3^-}(t_i) = \left[n^{bio}_{NO_3^-}(t_i) - n^{bio}_{NO_3^-}(t_0) \right] \times M_{NO_3^-} \quad (14)$$

where $n^{bio}_{NO_3^-}(t_i)$ and $n^{bio}_{NO_3^-}(t_0)$ are defined by expression 12 with $n^{bio}_{NO_3^-}(t_0)$ the value at the tube inlet.

Figure 8 shows the evolution of the nitrate transformation rate V_{trans} (Eq. 10) as a function of our estimate of the potential biofilm thickness b_{bio} (Eq. 7) for the batch

HESSD
11, 9829–9862, 2014

(black curve) and flow experiments (full blue, dashed green, dashdot magenta and dotted red curves). From the latter results, the batch experiment is characterized by a strong increase of the nitrate transformation rate when the biofilm thickness evolves from 0 to 8.8 µm, followed by a strong decrease when the biofilm thickness is larger than 8.8 µm. As expected for this case, biofilm growth is first fast and not limited by nitrate concentration; then, biofilm growth is limited by nutrient availability, as the total quantity of nitrate is consumed at the end of the experiment.

Results presented in Fig. 8 show that the beginning of the flow experiments is characterized by a similar strong linear increase of the nitrate transformation rate (dashed black line). The nitrate transformation rate differs from the latter behavior when the biofilm thickness reaches the values of 0.16 and 0.41 µm for the flow experiments v_1 and v_2, respectively, and the value of 1 µm for the flow experiments v_3 and v_4.

After the previously described linear increase, the nitrate transformation rate associated with the slowest flow velocity v_1 follows two distinguished behaviors. When the biofilm thickness is between 0.16 and 4.4 µm, the superposition of the large black and full blue curves shows that the relationship between the nitrate transformation rate and the biofilm thickness is similar for the batch experiment and the flow experiment v_1. When the biofilm thickness is larger than 4.4 µm, the behavior of the two latter experiments differs and the nitrate transformation rate is characterized by a relative stabilization for the flow experiment v_1.

Increasing the flow velocity from v_1 to v_2 implies that the initial linear increase of the nitrate transformation rate is observed until the biofilm thickness reaches the value of 0.41 µm (instead of 0.16 µm for the flow velocity v_1). When the biofilm thickness is larger than 0.41 µm, the flow experiment v_2 leads to a relative stabilization of the nitrate transformation rate characterized by small variations in comparison to the initial linear increase.

Finally, the flow experiments conducted with the two fastest flow velocities v_3 and v_4 lead to similar results. In both cases, the behavior of the nitrate transformation rate differs from the initial linear increase when the biofilm thickness reaches the value of

HESSD
11, 9829–9862, 2014

1 µm. When the biofilm thickness is larger than 1 µm, the nitrate transformation rate is characterized by a series of strong variations that oscillate around a similar threshold value.

5 Discussion

The evolution of the relationship between the nitrate transformation rate V_{trans} and the biofilm thickness b_{bio} for the batch and flow experiments (Fig. 8) enables us to extract information concerning the flow-velocity impact on reaction efficiency and on the related biofilm properties.

5.1 Differences and similarities between static and dynamic experiments

At the very beginning of the experiments, the relationship between V_{trans} and b_{bio} is similar for the four flow experiments (black dashed curve). This first short-time phase characterizes a phenomenon that initiates the reactive process, such as attachment of cells by adsorption on the tube walls, followed by a strong linear increase of the nitrate transformation rate related to biofilm growth. This fast evolution of the reaction efficiency characterizes a fast modification of the biofilm/fluid reactive contact area that is not flow-velocity dependent for the studied range of flow velocities.

Concerning the flow experiment v_1, the latter behavior is observed until the biofilm thickness reaches the estimated value of 0.16 µm. After this value, and considering $b_{bio}^{v_1}$ the critical biofilm thickness set at 4.4 µm, the relationship between V_{trans} and b_{bio} is similar for the batch experiment and the flow experiment v_1 when $b_{bio} < b_{bio}^{v_1}$. In opposition, when $b_{bio} > b_{bio}^{v_1}$, the nitrate transformation rate keeps increasing with the biofilm thickness for the static experiment whereas a relative stabilization is observed for the flow experiment. In terms of interactions between hydraulic conditions, biofilm properties and biological reactivity, the flow experiment v_1 is thus characterized by a first phase where the dynamic conditions do not impact the reaction efficiency

HESSD
11, 9829–9862, 2014

corresponding to a flow velocity too small to modify the structural properties of the biofilm during its development. In the second phase, the conditions of the dynamic experiment imply a stabilization of the biofilm reactivity that characterizes biofilm production/loss equilibrium where biofilm loss is driven by processes such as decay and erosion.

Concerning the flow experiments v_2, v_3 and v_4, the relationship between V_{trans} and b_{bio} clearly differs from the batch experiment during the entire experiment. The three experiments conducted with the fastest flow velocities are characterized first by a fast linear increase of the reactivity with the biofilm thickness, and then by a relative stabilization. During the initial linear increase and the beginning of the stabilization, the reaction efficiency is optimized under dynamic conditions conducted with large flow velocities since the values of V_{trans} observed for the flow experiments v_2, v_3 and v_4 are higher than the values observed for the batch experiment and the flow experiment v_1. However, the stabilization implies that the latter optimization breaks down when the biofilm thickness is larger than 4 µm where the batch experiment presents high values of V_{trans}.

5.2 Impact of flow velocity on reaction efficiency

Considering the same effective biofilm thickness b_{bio}, the high reaction efficiency observed at the beginning of the flow experiments v_2, v_3 and v_4 reveals an optimization of the biofilm/fluid reactive contact area due to specific hydraulic conditions. The latter behavior characterizes the impact of specific phenomena on the biofilm properties leading to an increase of its reactivity under dynamic conditions.

In relation to previous studies, it has been demonstrated that hydraulic constraints can imply an increase of the biofilm height (Hornemann et al., 2009) due to the presence of secondary velocities that are perpendicular to the deposit surface and that generate an upward shear force in the downstream side of the biofilm (Vo and Heys, 2011). It results in a higher and heterogeneous biofilm structure that optimizes the biofilm/fluid contact area and thus the efficiency of the denitrification process. In addition, it has

HESSD
11, 9829–9862, 2014

been demonstrated that applying fast advective flows parallel to the deposit surface leads to heterogeneous deposits of bacteria along the tube surface (Yu et al., 1999). The latter phenomenon results in the formation of patch structures that have been observed during the experiments (Fig. 4a) and where the biofilm/fluid contact area is optimized in comparison to continuous structures.

It is important to notice that these conclusions are in contradiction with some previous studies showing that fluid shear tends to compress the biofilm towards the surface (Picioreanu et al., 2001; van Loosdrecht et al., 2002; Wanner et al., 1995). However, the biofilm models and experiments of the latter studies are based on assumptions that differ from our experiment, such as homogeneous and isotropic biofilm assumption (Picioreanu et al., 2001) or experimental conditions where flow is applied to a biofilm grown without flow (Wanner et al., 1995). This demonstrates the complexity of the relationship between biofilm properties and hydrodynamic parameters, the importance of model assumptions and experimental conditions, and the critical differences of biofilm properties when the biofilm grows under static or dynamic conditions.

5.3 Impact of flow velocity on reaction stabilization

After reaching its maximum value, the nitrate transformation rate oscillates around the threshold value reached when the biofilm thickness is equal to 0.44 µm for the flow velocity v_2 and 1 µm for the flow velocities v_3 and v_4. The observed successions of increase/decrease cycles of the nitrate transformation rate characterize repeated variations of the biofilm/fluid reactive contact area, and thus of the biofilm structural properties. Increasing the flow velocity from v_2 to v_3 implies that (1) the transition between the linear increase and the relative stabilization is observed at a larger value of the biofilm thickness, (2) the nitrate transformation rate oscillates around a larger threshold value and (3) the variations of the nitrate transformation rate around the latter threshold value are larger (which is observed as well when increasing the flow velocity from v_3 to v_4).

The transition from a linear increase to a relative stabilization starts by a slow decrease of the nitrate transformation rate after reaching its maximum value. The latter

HESSD
11, 9829–9862, 2014

decrease is observed when the biofilm thickness evolves from 1.4 to 3.2 µm for the flow velocities v_3 and v_4 and characterizes a progressive variation of the biofilm structural properties from an optimal configuration to a less reactive configuration. The transition from patches (Fig. 4a) to continuous structures (Fig. 4b) observed during the experiments is characteristic of the latter behavior where the patch structures optimize the biofilm/fluid contact area (and thus the reactivity) in comparison to continuous structures and where the transition from the first to the second kind of structures occurs progressively with new deposits and/or bacterial growth that fill the spaces between patches.

The large oscillations of the nitrate transformation rate observed for the flow velocities v_3 and v_4 may characterize fast and important variations of the biofilm structural properties due to flow-dependent phenomena such as detachment and reattachment. The latter experiments correspond to hydraulic conditions with fast flow velocities that can imply a strong heterogeneity of the structures due to upward shear forces and heterogeneous deposits (as explained in the previous section). In relation to previous studies, it has been shown that the formation of heterogeneous structures implies the presence of protuberances on the biofilm surface where microorganisms grow faster and form tower-like colonies (Picioreanu et al., 1998). It leads to the presence of cavities where nutrients are not easily accessible and enhances the fragility of the biofilm, and thus potential detachment. In addition, for strong shear stress (correlated to fast flows), the potential detachment promotes biofilm spatial heterogeneity by reattachment (Stewart, 1993). The observed succession of decreases and increases might thus be due to detachments and reattachments related to a strong heterogeneity of the biofilm structures.

This study presents an interesting experiment to characterize the influence of flow velocity on biogeochemical reactions where the impact of flow velocity on reactivity is demonstrated. We further propose a framework for its interpretation. Unfortunately it was not possible to continuously monitor and characterize the biofilm due to technical constraints. This should be performed in further studies on the topic. However, this

HESSD
11, 9829–9862, 2014

study provides interesting insights on the interest of dynamic experiments over static experiments as well as on the complexity of reactivity in dynamic conditions.

6 Conclusions

The presented experiment and analytical framework aim to characterize biochemical reactivity in the case of mobile/immobile electron acceptor/donor under dynamic conditions to assess the influence of flow velocity on biologically constrained reaction rates. This is done through an original experiment where nitrate-rich water passes continuously through plastic tubes at several flow velocities (from 6.2 to 35 mm min^{-1}). Flow velocity appears to be a key factor for reaction efficiency and stability as experiments conducted with the largest flow velocities are characterized by a fast increase of the reactivity rate until reaching a threshold where strong oscillations are observed. The latter behavior characterizes an optimization of the biofilm/fluid reactive contact area related to cell attachment and biofilm growth followed by equilibrium between bacteria development and flow impact on the biofilm structures subject to decay/detachment phenomena. In opposition, the same experiment conducted with a small flow velocity leads to a slow increase of the reactivity rate until reaching a stable threshold value.

The different behaviors observed between static and dynamic experiments show the relevance of dynamic experiments for the understanding and characterization of biogeochemical processes in natural media. The presented dynamic experiments demonstrate that the presence of flow impacts the reactivity rate behavior at different steps of the biofilm development with step-dependent effects of the flow intensity. In natural environments characterized by a broad range of flow velocities, such as soils with macropores or fractured aquifers, the resulting heterogeneous reaction rates might impact the global reactivity of the site. In addition, dynamic conditions related to long-time pumping for water exploitation seem to have an impact on biogeochemical reactivity as observed in the Ploemeur site (Tarits et al., 2006) by enhancing the long-term reactivity at the site scale. For fractured media, most of the denitrification process should occur

HESSD
11, 9829–9862, 2014

within the fractures, as they are opened channels favorable to microbial development and nutrient (i.e. nitrates) circulation (Johnson et al., 1998) where the electron donor, such as pyrite, is present as a solid phase.

The presented study is a step for the understanding of heterogeneous and velocity-dependent reactivity in both porous and fractured media. Although this experiment was designed with the example of denitrification in synthetic conditions, observations and conclusions should be easily transposable to other applications.

Acknowledgements. The French National Research Agency ANR is acknowledged for its financial funding through the MOHINI project (ANR-07-VULN-008) as well as The National Observatory for Research in Environment H+ (SNO H+) for the support of the field data investigations. Financial support was also provided by the EU-RDF INTERREG IVA France (Channel) – England program (Climawat project).

References

Ayraud, V., Aquilina, L., Pauwels, H., Labasque, T., Pierson-Wickmann, A.-C., Aquilina, A.-M., and Gallat, G.: Physical, biogeochemical and isotopic processes related to heterogeneity of a shallow crystalline rock aquifer, Biogeochemistry, 81, 331–347, doi:10.1007/s10533-006-9044-4, 2006.

Bekins, B.: Preface – groundwater and microbial processes, Hydrogeol. J., 8, 2–3, doi:10.1007/s100400050002, 2000.

Beyenal, H. and Lewandowski, Z.: Combined effect of substrate concentration and flow velocity on effective diffusivity in biofilms, Water Res., 34, 528–538, doi:10.1016/S0043-1354(99)00147-5, 2000.

Bougon, N., Aquilina, L., Briand, M. P., Coedel, S., and Vandenkoornhuyse, P.: Influence of hydrological fluxes on the structure of nitrate-reducing bacteria communities in a peatland, Soil Biol. Biochem., 41, 1289–1300, doi:10.1016/j.soilbio.2009.03.015, 2009.

Characklis, W. G.: Fouling biofilm development: a process analysis, Biotechnol. Bioeng., 23, 1923–1960, doi:10.1002/bit.260230902, 1981.

HESSD
11, 9829–9862, 2014

Clément, J.-C., Aquilina, L., Bour, O., Plaine, K., Burt, T. P., and Pinay, G.: Hydrological flowpaths and nitrate removal rates within a riparian floodplain along a fourth-order stream in Brittany (France), Hydrol. Process., 17, 1177–1195, doi:10.1002/hyp.1192, 2003.

De Beer, D., Stoodley, P., and Lewandowski, Z.: Liquid flow and mass transport in heterogeneous biofilms, Water Res., 30, 2761–2765, doi:10.1016/S0043-1354(96)00141-8, 1996.

Ergas, S. and Reuss, A.: Hydrogenotrophic denitrification of drinking water using a hollow fibre membrane bioreactor, J. Water Supply Res. T., 50, 161–171, 2001.

Ergas, S. J. and Rheinheimer, D. E.: Drinking water denitrification using a membrane bioreactor, Water Res., 38, 3225–3232, doi:10.1016/j.watres.2004.04.019, 2004.

Garny, K., Neu, T. R., and Horn, H.: Sloughing and limited substrate conditions trigger filamentous growth in heterotrophic biofilms-Measurements in flow-through tube reactor, Chem. Eng. Sci., 64, 2723–2732, doi:10.1016/j.ces.2009.03.009, 2009.

Hamlin, H. J., Michaels, J. T., Beaulaton, C. M., Graham, W. F., Dutt, W., Steinbach, P., Losordo, T. M., Schrader, K. K., and Main, K. L.: Comparing denitrification rates and carbon sources in commercial scale upflow denitrification biological filters in aquaculture, Aquacult. Eng., 38, 79–92, doi:10.1016/j.aquaeng.2007.11.003, 2008.

Hiscock, K. M., Lloyd, J. W., and Lerner, D. N.: Review of natural and artificial denitrification of groundwater, Water Res., 25, 1099–1111, doi:10.1016/0043-1354(91)90203-3, 1991.

Hornemann, J. A., Codd, S. L., Fell, R. J., Stewart, P. S., and Seymour, J. D.: Secondary flow mixing due to biofilm growth in capillaries of varying dimensions, Biotechnol. Bioeng., 103, 353–360, doi:10.1002/bit.22248, 2009.

Jiménez-Martínez, J., Longuevergne, L., Le Borgne, T., Davy, P., Russian, A., and Bour, O.: Temporal and spatial scaling of hydraulic response to recharge in fractured aquifers: insights from a frequency domain analysis, Water Resour. Res., 49, 3007–3023, doi:10.1002/wrcr.20260, 2013.

Johnson, A. C., Hughes, C. D., Williams, R. J., and Chilton, P. J.: Potential for aerobic isoproturon biodegradation and sorption in the unsaturated and saturated zones of a chalk aquifer, J. Contam. Hydrol., 30, 281–297, doi:10.1016/S0169-7722(97)00048-X, 1998.

Khan, I. A. and Spalding, R. F.: Enhanced in situ denitrification for a municipal well, Water Res., 38, 3382–3388, doi:10.1016/j.watres.2004.04.052, 2004.

Kornaros, M. and Lyberatos, G.: Kinetics of aerobic growth of a denitrifying bacterium, pseudomonas denitrificans, in the presence of nitrates and/or nitrites, Water Res., 31, 479–488, doi:10.1016/S0043-1354(96)00288-6, 1997.

HESSD
11, 9829–9862, 2014

Korom, S. F.: Natural denitrification in the saturated zone: a review, Water Resour. Res., 28, 1657–1668, doi:10.1029/92WR00252, 1992.
Lau, Y. L. and Liu, D.: Effect of flow rate on biofilm accumulation in open channels, Water Res., 27, 355–360, doi:10.1016/0043-1354(93)90034-F, 1993.
Leray, S., de Dreuzy, J.-R., Bour, O., Labasque, T., and Aquilina, L.: Contribution of age data to the characterization of complex aquifers, J. Hydrol., 464–465, 54–68, doi:10.1016/j.jhydrol.2012.06.052, 2012.
Lewandowski, Z., Beyenal, H., Myers, J., and Stookey, D.: The effect of detachment on biofilm structure and activity: the oscillating pattern of biofilm accumulation, Water Sci. Technol., 55, 429–436, doi:10.2166/wst.2007.287, 2007.
Marazioti, C., Kornaros, M., and Lyberatos, G.: Kinetic modeling of a mixed culture of Pseudomonas Denitrificans and Bacillus subtilis under aerobic and anoxic operating conditions, Water Res., 37, 1239–1251, doi:10.1016/S0043-1354(02)00463-3, 2003.
McCarty, P. L.: Stoichiometry of Biological Reactions, Dept. of Civil Engineering, Stanford, Stanford University, 1972.
Mohee, R., Unmar, G. D., Mudhoo, A., and Khadoo, P.: Biodegradability of biodegradable/degradable plastic materials under aerobic and anaerobic conditions, Waste Manage., 28, 1624–1629, doi:10.1016/j.wasman.2007.07.003, 2008.
Picioreanu, C., van Loosdrecht, M., and Heijnen, J.: Mathematical modeling of biofilm structure with a hybrid differential-discrete cellular automaton approach, Biotechnol. Bioeng., 58, 101–116, doi:10.1002/(SICI)1097-0290(19980405)58:1<101:AID-BIT11>3.0.CO;2-M, 1998.
Picioreanu, C., van Loosdrecht, M., and Heijnen, J.: Two-dimensional model of biofilm detachment caused by internal stress from liquid flow, Biotechnol. Bioeng., 72, 205–218, 2001.
Ruelleu, S., Moreau, F., Bour, O., Gapais, D., and Martelet, G.: Impact of gently dipping discontinuities on basement aquifer recharge: an example from Ploemeur (Brittany, France), J. Appl. Geophys., 70, 161–168, doi:10.1016/j.jappgeo.2009.12.007, 2010.
Sengupta, S. and Ergas, S.: Autotrophic biological denitrification with elemental sulfur or hydrogen for complete removal of nitrate-nitrogen from a septic system wastewater, NOAA/UNH Cooperative Institute for Coastal and Estuarine Environmental Technology (CICEET), Durham, New Hampshire, USA, 2006.
Shah, A. A., Hasan, F., Hameed, A., and Ahmed, S.: Biological degradation of plastics: a comprehensive review, Biotechnol. Adv., 26, 246–265, doi:10.1016/j.biotechadv.2007.12.005, 2008.

HESSD
11, 9829–9862, 2014

Sinke, A. J. C., Dury, O., and Zobrist, J.: Effects of a fluctuating water table: column study on redox dynamics and fate of some organic pollutants, J. Contam. Hydrol., 33, 231–246, doi:10.1016/S0169-7722(98)00072-2, 1998.

Spalding, R. and Exner, M.: Occurrence of nitrate in groundwater – a review, J. Environ. Qual., 22, 392–402 , 1993.

Stewart, P. S.: A model of biofilm detachment, Biotechnol. Bioeng., 41, 111–117, doi:10.1002/bit.260410115, 1993.

Stoodley, P., De Beer, D., and Lewandowski, Z.: Liquid flow in biofilm systems, Appl. Environ. Microb., 60, 2711–2716, 1994.

Sturman, P. J., Stewart, P. S., Cunningham, A. B., Bouwer, E. J., and Wolfram, J. H.: Engineering scale-up of in situ bioremediation processes: a review, J. Contam. Hydrol., 19, 171–203, doi:10.1016/0169-7722(95)00017-P, 1995.

Tarits, C., Aquilina, L., Ayraud, V., Pauwels, H., Davy, P., Touchard, F., and Bour, O.: Oxido-reduction sequence related to flux variations of groundwater from a fractured basement aquifer (Ploemeur area, France), Appl. Geochem., 21, 29–47, doi:10.1016/j.apgeochem.2005.09.004, 2006.

Thullner, M., Zeyer, J., and Kinzelbach, W.: Influence of microbial growth on hydraulic properties of pore networks, Transport Porous Med., 49, 99–122, doi:10.1023/A:1016030112089, 2002.

Tompkins, J., Smith, S., Cartmell, E., and Wheater, H.: In-situ bioremediation is a viable option for denitrification of Chalk groundwaters, Q. J. Eng. Geol. Hydroge., 34, 111–125, 2001.

van Loosdrecht, M. C. M., Heijnen, J. J., Eberl, H., Kreft, J., and Picioreanu, C.: Mathematical modelling of biofilm structures, A. van Leeuw. J. Microb., 81, 245–256, doi:10.1023/A:1020527020464, 2002.

Vo, G. D. and Heys, J.: Biofilm deformation in response to fluid flow in capillaries, Biotechnol. Bioeng., 108, 1893–1899, doi:10.1002/bit.23139, 2011.

von Gunten, U. and Zobrist, J.: Biogeochemical changes in groundwater-infiltration systems: column studies, Geochim. Cosmochim. Acta, 57, 3895–3906, doi:10.1016/0016-7037(93)90342-T, 1993.

Wanner, O., Cunningham, A., and Lundman, R.: Modeling biofilm accumulation and mass-transport in a porous-medium under high substrate loading, Biotechnol. Bioeng., 47, 703–712, doi:10.1002/bit.260470611, 1995.

HESSD
11, 9829–9862, 2014

Williamson, K. and McCarty, P. L.: A model of substrate utilization by bacterial films, J. Water Pollut. Con. F., 48, 9–24, 1976.
Yu, L., Xuefu, Y., and Dalin, G.: Biofilm formation and control in flowing system, Huanjing Kexue, 20, 98–99, 1999.

HESSD
11, 9829–9862, 2014

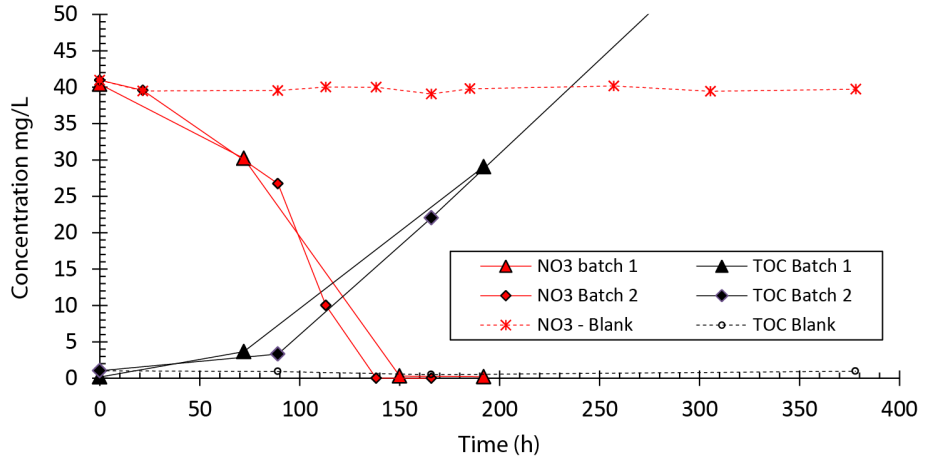

Figure 1. Evolution of nitrates and total organic carbon in batch experiments. For the Bath 2 a value TOC of 76.8 mg L^{-1} has been recorded after 378 h.

HESSD
11, 9829–9862, 2014

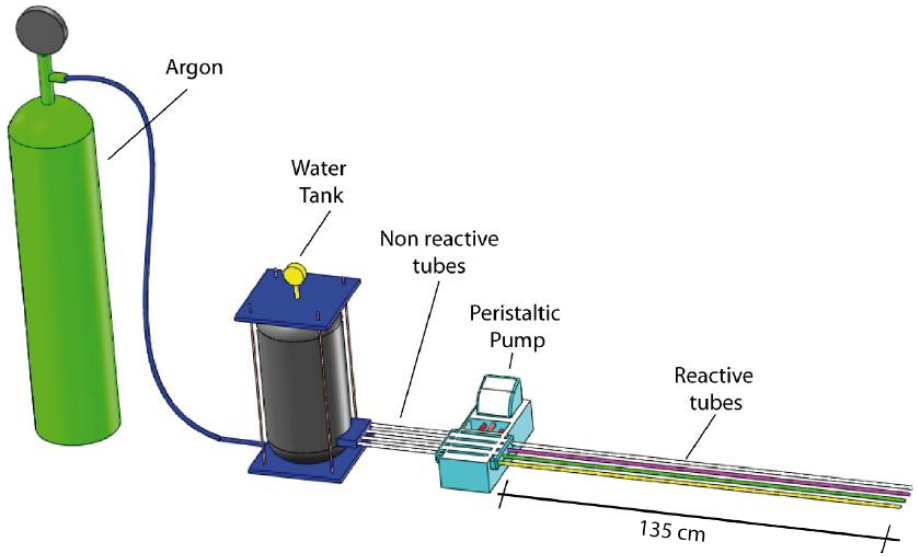

Figure 2. Schematic representation of the experimental setup. The water is maintained under an argon atmosphere in a tank. The water passes through non-reactive tubes from the tank to the peristaltic pump and then through reactive tubes at different velocities. For each experiment, a non-reactive tube of the same length is used in parallel to assess the inlet concentration.

HESSD
11, 9829–9862, 2014

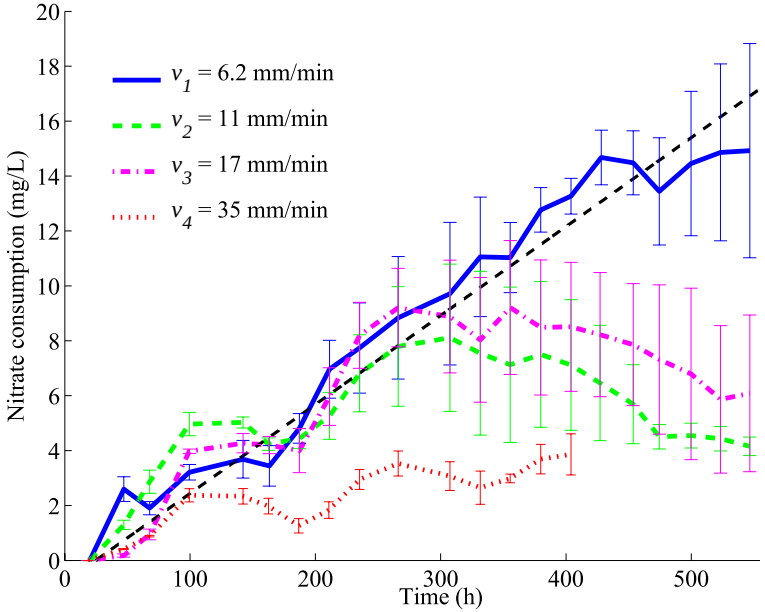

Figure 3. Temporal evolution of the nitrate consumption $\Delta C_{NO_3^-}(t)$ ($mg\,L^{-1}$) for the dynamic experiments conducted with the flow velocities v_1 (full blue curve), v_2 (dashed green curve), v_3 (dashdot magenta curve) and v_4 (dotted red curve). The presented values are the averages of 3 replicates where error bars represent the mean square deviation.

HESSD
11, 9829–9862, 2014

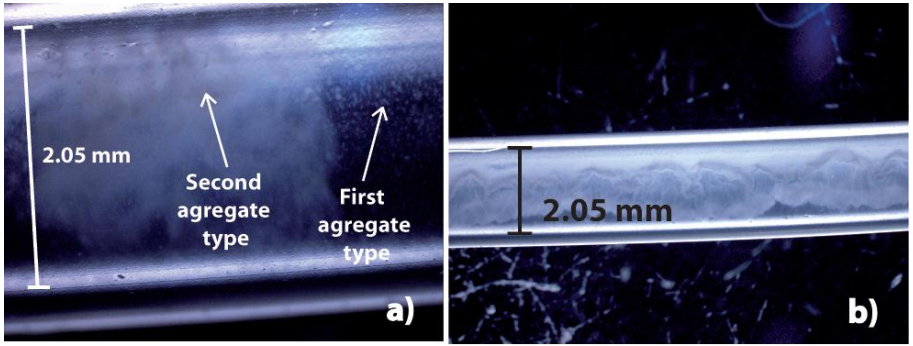

Figure 4. Biofilm development in the tubes as **(a)** millimeter and centimeter long clusters and **(b)** continuous biofilm.

HESSD
11, 9829–9862, 2014

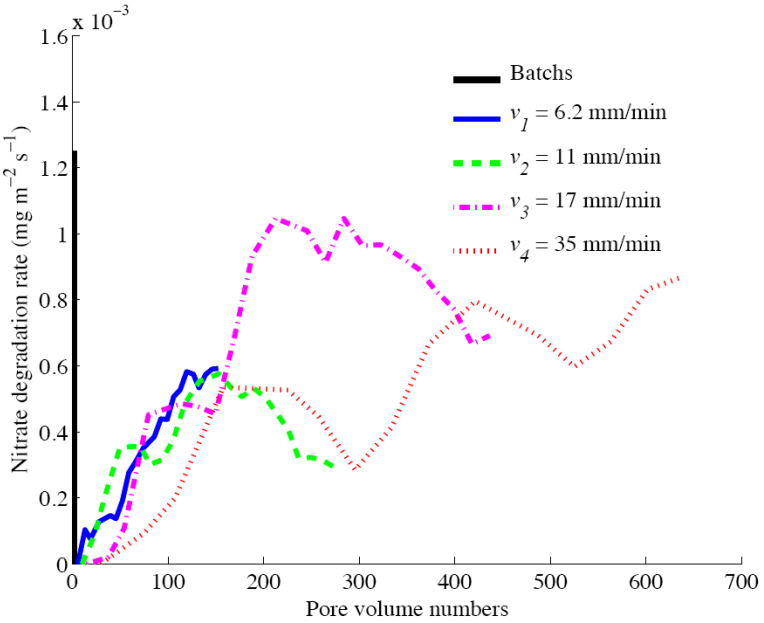

Figure 5. Nitrate degradation rate versus the number of pore volumes for the batch (black curve) and tube experiments conducted with the flow velocities v_1 (full blue curve), v_2 (dashed green curve), v_3 (dashdot magenta curve) and v_4 (dotted red curve).

HESSD
11, 9829–9862, 2014

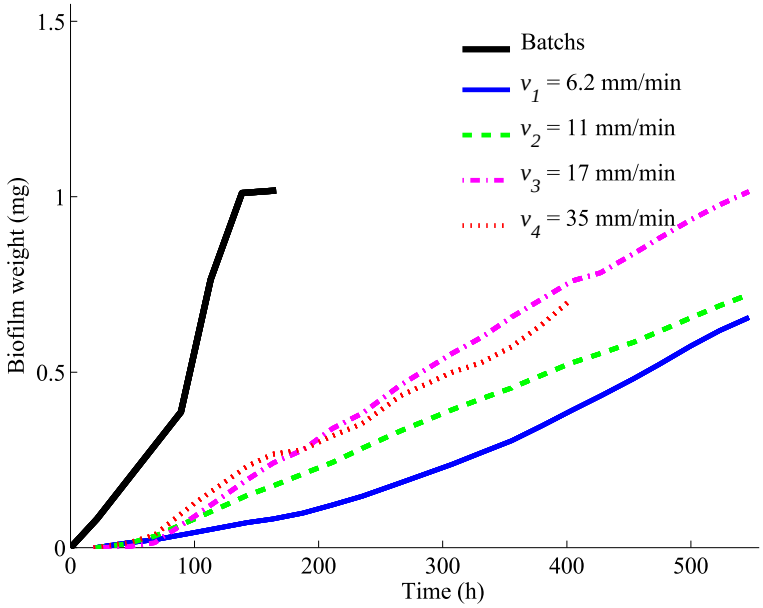

Figure 6. Temporal evolution of the total biofilm weight $\overline{m_{bio}}$ (mg) for the batch (black curve) and tube experiments conducted with the flow velocities v_1 (full blue curve), v_2 (dashed green curve), v_3 (dashdot magenta curve) and v_4 (dotted red curve).

HESSD
11, 9829–9862, 2014

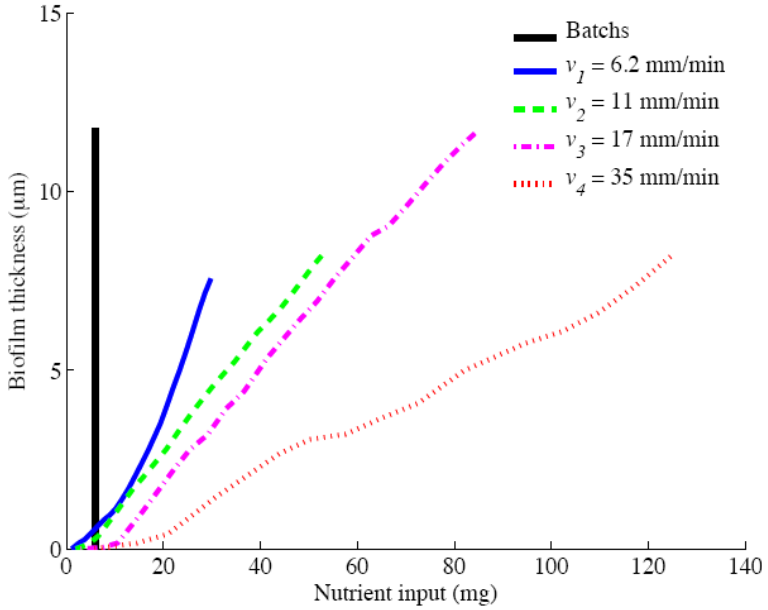

Figure 7. Evolution of the biofilm thickness b_{bio} (µm) with the nutrient input N_{input} (mg) for the batch (black curve) and tube experiments conducted with the flow velocities v_1 (full blue curve), v_2 (dashed green curve), v_3 (dashdot magenta curve) and v_4 (dotted red curve).

HESSD
11, 9829–9862, 2014

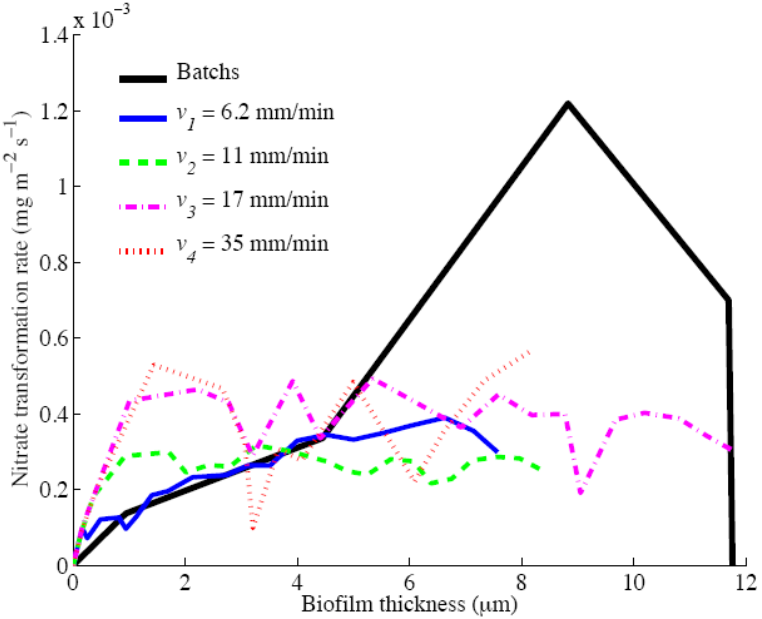

Figure 8. Evolution of the nitrate transformation rate V_{trans} (mg m^{-2} s^{-1}) with the biofilm thickness b_{bio} (µm) for the batch (black curve) and tube experiments conducted with the flow velocities v_1 (full blue curve), v_2 (dashed green curve), v_3 (dashdot magenta curve) and v_4 (dotted red curve).

HESSD
11, 9829–9862, 2014